Where Does Dense Water Sink? A Subpolar Gyre Example*

MICHAEL A. SPALL AND ROBERT S. PICKART

Department of Physical Oceanography, Woods Hole Oceanographic Institution, Woods Hole, Massachusetts

(Manuscript received 21 July 1999, in final form 1 June 2000)

ABSTRACT

It is proposed that a dominant component of the downwelling limb of the thermohaline circulation takes place in regions where convective mixing is found adjacent to steep topography. A simple theoretical estimate of the overturning forced by such boundary convection is derived that depends only on the properties of the oceanic mixed layer along the boundary. Scaling estimates indicate that sinking forced by boundary convection is an order of magnitude greater than sinking in the open ocean resulting from large-scale dynamics or baroclinic instability of deep convective sites. Recent hydrographic observations in the Labrador Sea are used to estimate the downwelling due to these different mechanisms and support the notion that boundary sinking dominates. The theory compares well with the overturning rates diagnosed in a noneddy-resolving general circulation model over a wide range of parameters. As a direct consequence of these dynamics, the high-latitude hydrography and overturning circulation in the model are very sensitive to the presence of cyclonic rim currents. Lateral density advection by the rim currents in the subpolar gyre increases the stratification and limits the mixing near the boundaries, thus reducing the maximum downwelling. As a result, most of the high-latitude meridional heat transport is carried by the horizontal circulation instead of the overturning circulation. Such rim currents are found in different configurations of the model, including 1) a continental slope and standard diffusion parameters and 2) zero horizontal diffusion and a flat bottom.

1. Introduction

The meridional overturning circulation is of fundamental importance to the global climate system. Water in the upper ocean flows from low latitudes toward the poles, where it is cooled and heat is released into the atmosphere. The modified (more dense) water is then returned to middle and low latitudes as intermediate and deep water masses. The mass flux in the meridional plane is thought to be closed by upwelling, primarily at middle and low latitudes. While this scenario is no doubt correct in the broadest sense, a better understanding of where these vertical mass fluxes take place, and of what physical processes control the location and amplitude of the vertical exchange, is necessary if we are to understand the ocean's circulation and its role in climate. Recent results from high-resolution microstructure profilers (Polzin et al. 1997) and tracer release experiments (Ledwell et al. 1993) are beginning to shed light on where these deep waters are upwelled into the upper ocean (and where they are not). This paper attempts to provide a dynamical framework for understanding where the high-latitude downwelling takes place and what constrains its magnitude.

There has been a great deal of recent interest in the meridional overturning circulation and its subsequent heat transport. Many low-resolution modeling studies have focused on the relationship between the overturning rate and the model paramerizations of unresolved processes such as vertical mixing of density, air–sea exchange, and exchange with other basins (e.g., Bryan 1987; Marotzke 1997; Döscher et al. 1994). Attempts to scale the overturning strength with model and atmospheric parameters have achieved some level of success (Bryan 1987; Colin de Verdiere 1988; Marotzke 1997; Zhang et al. 1999, Park and Bryan 2000). Low-resolution models have also shown that the very nature of the thermohaline circulation can be strongly time dependent—experiencing total collapse, periodic oscillations, or chaotic oscillations (Stommel 1961; Bryan 1987; Weaver et al. 1993). The variability of the overturning circulation and associated meridional heat transport in these models is associated with the shutting down of deep convection and sinking at high latitudes, although the dynamics that control these sinking rates and regions are not well understood. A recent study by Marotzke and Scott (1999) has begun to explore the dynamics of sinking regions and to distinguish down-

* Woods Hole Oceanographic Institution Contribution Number 10103.

Corresponding author address: Michael A. Spall, Woods Hole Oceanographic Institution, Woods Hole, MA 02543.
E-mail: mspall@whoi.edu, rpickart@whoi.edu

welling from convective mixing. Many of these models are configured in the most simple way possible by making use of a flat bottom and forcing the circulation with zonally averaged properties. The resulting circulations, particularly in the subpolar gyre, can be very unrealistic when compared to observations.

There have also been numerous studies using both low- and high-resolution models that are configured in realistic domains and are forced with realistic air–sea fluxes. The exchanges with other basins are often parameterized in these calculations by restoring the temperature and salinity fields toward climatological values near the meridional boundaries (Bryan and Holland 1989; Böning et al. 1996). The circulation and density structure in these models are generally much more realistic than are found in the flat bottom, idealized calculations. Recent advances in the parameterization of mesoscale processes have resulted in meridional heat transports and overturning circulations that are in general agreement with observational estimates (Böning et al. 1995). However, many aspects of the subpolar circulation and meridional heat transport in basin-scale models are sensitive to how the exchanges with high latitude basins are parameterized within the buffer zones (Döscher et al. 1994; Böning et al. 1996). In part because of this sensitivity to boundary conditions, little attention has been paid in the analysis of these models to the dynamics that control the downwelling limb of the thermohaline circulation.

In the present study, we seek to develop a basic understanding of what determines the regions and rate of sinking at high latitudes. While the discussion is formulated in the context of a subpolar gyre circulation, the results are relevant to the general problem of dense water-sinking, such as occurs in the subarctic seas or semienclosed seas (i.e., the Nordic seas, the Mediterranean Sea, or Red Sea) or near the west coast of Australia (Godfrey and Ridgway 1985). Some aspects of this anaysis will involve convective mixing, but our primary focus is on the downward mass flux, not on the processes of water mass transformation. The sinking mechanisms that are considered in this study include: diapycnal mixing near steep topography, large-scale open ocean sinking, baroclinic instability of convective sites, Ekman convergence, and the subduction at colliding western boundary currents.

2. Cooling spirals and downwelling

Because we anticipate that sinking at high latitudes may result when heat is lost to the atmosphere and the water is made more dense, our analysis begins by considering the thermodynamic balances within a mixed layer subject to cooling. In a steady state with no horizontal diffusion, the horizontal advection of density is balanced by buoyancy loss to the atmosphere and convective mixing, represented here as Q (positive values represent cooling):

$$u\rho_x + v\rho_y = Q. \tag{1}$$

Within the mixed layer $\rho_z = 0$ and there is no contribution from vertical advection. The cooling of parcels requires that the flow cross isopycnals from light to dense. The advection of density is achieved by the depth-averaged flow within the mixed layer because the nonlinear terms cancel for the vertically sheared geostrophic flow. If the horizontal flow with magnitude V and direction θ (relative to east) is assumed to be in geostrophic balance, then (1) may be manipulated to represent the rotation of the velocity vector with depth as

$$\theta_z = -\frac{gQ}{f\rho_0 V^2}, \tag{2}$$

where f is the Coriolis parameter, g is the gravitational acceleration, and ρ_0 is a reference density of seawater [similar derivations may be found in Schott and Stommel (1978), Stommel (1979), and Spall (1992)]. For regions in which convective mixing is increasing the density of the ocean, the velocity vector will spiral counterclockwise with depth. Such rotation with depth was inferred from hydrographic data in the subpolar gyre by Luyten et al. (1985) and Stommel (1979). The direction of flow as a function of depth may be found by integrating (2),

$$\theta(z) = \theta_0 - \frac{gQz}{f\rho_0 V^2}. \tag{3}$$

For simplicity, we have assumed here that the magnitude of the velocity vector is constant in depth, in general agreement with the observations in the interior of the subpolar gyre (Stommel 1979) and near the boundaries (Pickart and Torres 1998). This expression is valid throughout the basin where the flow is in geostrophic balance. In the open ocean, the flow can satisfy geostrophic and thermodynamic balances by remaining essentially horizontal and spiraling with depth. This is consistent with the velocity structure and buoyancy forcing inferred by Luyten et al. (1985) in the eastern North Atlantic subpolar gyre.

The physical interpretation of (3) is straightforward. Flow perpendicular to the isopycnals is required in order to balance the heat loss to the atmosphere; however, this flow has no vertical shear. The flow component parallel to the isopycnals within the mixed layer must have a vertical shear in order to satisfy thermal wind balance. Thus, the direction of the flow must rotate counterclockwise with depth. The assumption that V is constant is reasonable provided that the flow perpendicular to the isopycnals is larger that the thermal wind associated with the horizontal density gradient within the mixed layer.

a. Cooling near a boundary

Large vertical velocities can result from the cooling spiral if the cooling takes place adjacent to a boundary

or steep topography. In a general sense, this is analogous to upwelling that results when wind stress forces an Ekman spiral adjacent to a coast. In the present case the spiral, forced by buoyancy loss to the atmosphere and geostrophic dynamics, is distributed over the depth of the mixed layer. However, as in the case of coastal upwelling, mass continuity requires large vertical velocities next to the boundary. Without loss of generality, the following discussion is formulated in the context of downwelling near a northern boundary. It should be clear that the results are easily applied to any boundary where cooling is taking place.

The net downwelling that results from a cooling spiral near a northern boundary can be calculated by integrating the meridional velocity from the western boundary to the eastern boundary between the surface and the level of no meridional motion. The reference angle θ_0 in (3) is related to the level of no meridional motion and, indirectly, the northward mass flux. The level of no motion for the zonally integrated flow may be calculated by requiring that the net meridional mass flux integrated over the mixed layer h and the zonal extent of the basin L_x is zero. This is equivalent to assuming that the vertical velocity out of the base of the mixed layer is zero, or that diapycnal mixing below the mixed layer is weak. The analysis is simplified if it is assumed that the mixed layer depth is constant along the boundary, although this need not be the case. It would be straightforward to carry out the integration if the density and mixed layer depth were known as a function of position along the boundary, but the basic result is qualitatively unchanged and most clearly demonstrated when considering the uniform mixed layer case. For a geostrophic flow, it is easy to show that the level of no motion for the zonally averaged flow within the mixed layer is at depth $z = h/2$.

Assuming that the horizontal velocity adjacent to a lateral boundary is oriented nearly parallel to the boundary, consistent with the observations of Pickart and Torres (1998) in the subpolar North Atlantic, the meridional velocity near the northern boundary may be approximated by the first term in a series expansion for $\sin\theta$ as $v \approx \theta V$. Taking the level of no motion to be the same as for the zonally averaged flow, Eq. (3) may then be used to obtain the meridional velocity adjacent to the northern boundary as a function of depth,

$$v(z) \approx \frac{ghQ}{2\rho_0 f V}\left(1 - \frac{2z}{h}\right). \tag{4}$$

In a region of cooling $Q > 0$ so that the meridional velocity is northward in the upper mixed layer ($z < h/2$) and southward in the lower mixed layer, with linear vertical shear. The meridional transport per unit depth is calculated by integrating the meridional velocity from west to east:

$$\int_0^{L_x} v\, dx = \frac{gh}{2\rho_0 f}\left(1 - \frac{2z}{h}\right)\int_0^{L_x} \frac{Q}{V}\, dx. \tag{5}$$

This expression is simplified if it is recognized that near the northern boundary the dominant balance in the density equation is between the advection of density along the boundary and the cooling supplied by convective mixing, $V\rho_x \approx Q$. This simple zonal balance arises because it is the velocity averaged over the depth of the mixed layer that contributes to the density advection, and the depth-averaged velocity perpendicular to the boundary vanishes as the boundary is approached. The meridional transport per unit depth may then be written in terms of $\Delta\rho_B$, the change in density along the boundary between $x = 0$ and $x = L_x$:

$$\int_0^{L_x} v\, dx = \frac{gh\Delta\rho_B}{2\rho_0 f}\left(1 - \frac{2z}{h}\right). \tag{6}$$

Recall that the meridional velocity has linear vertical shear with a level of no motion at the middle of the mixed layer. The magnitude of the shear is simply the thermal wind resulting from geostrophy. Mass continuity requires that the zonal integral of the vertical velocity balance this mass flux into the northern boundary region. Because the meridional velocity has linear vertical shear, the vertical velocity will increase quadratically with depth within the mixed layer to a maximum value at $z = h/2$. The total meridional overturning M_B forced by boundary convection is found by integrating the meridional transport per unit depth down to the middle of the mixed layer,

$$M_B = \int_0^{h/2}\int_0^{L_x} v\, dx\, dz = \frac{g\Delta\rho_B h^2}{8\rho_0 f}. \tag{7}$$

This overturning rate may be interpreted as the zonal integral of the northward geostrophic velocity with a level of no motion at the midpoint of the mixed layer. In fact, this expression could have been obtained directly from geostrophy and mass continuity without consideration of the thermodynamic balances. However, we felt it useful to start from the density equation in order to demonstrate that the velocity structure along the boundary is a direct consequence of lateral advection and cooling within the mixed layer. Note that the total sinking rate is related only to the properties of the mixed layer adjacent to the boundary. It does not depend explicitly on the dynamics or thermodynamics away from the boundary, only in that they are important in determining the properties along the boundary. Somewhat surprisingly, M_B also does not depend explicitly on the surface heat flux, length of the boundary, or magnitude of the advection along the boundary, although they clearly influence $\Delta\rho_B$ and h.

The diagnostic approach taken here complements the approach taken by many previous investigators whereby the overturning rate is scaled directly from known model parameters, that is, vertical diffusivity and the atmo-

spheric temperature (Bryan and Cox 1967; Bryan 1987; Colin de Verdiere 1988; Marotzke 1997; Zhang et al. 1999; Park and Bryan 2000). The form of (7) is the same as has been derived from classical scaling arguments originating with Robinson and Stommel (1959) and Bryan and Cox (1967); a recent review is given by Park and Bryan (2000). The interpretation is different, however, as our vertical scale is the mixed layer depth along the boundary instead of the vertical scale of the thermocline and the density variation is set by the properties of the mixed layer in the subpolar gyre rather than the basin-scale sea surface temperature. The importance of density variations in the subpolar gyre was also emphasized in the recent study by Samelson and Vallis (1997). We emphasize here that our result is not a scaling but rather a quantitative estimate; there are no empirical factors in (7).

The mixed layer depth is controlled primarily by the balance between atmospheric forcing and oceanic advection. Oceanic advection and sea surface temperature are indirectly influenced-by more subtle and sometimes nonlocal processes such as vertical mixing in the ocean interior or constraints imposed by bottom topography. Although these model parameters do not appear explicitly in our estimate of the overturning rate, they are important in determining the properties along the northern boundaries and, hence, are indirectly included in (7).

b. Comparison with other sinking mechanisms

The mechanism outlined in the preceeding section is only one process that may lead to sinking within regions of buoyancy loss. Deep mixing is found throughout the high-latitude seas and has often been thought to correspond to regions of downward mass flux (i.e., Dietrich et al. 1980; Schmitz and McCartney 1993). However, as pointed out by Marotzke and Scott (1999) and Mauritzen and Häkkinen (1999), the regions of deep mixing need not coincide with regions of net downwelling. This will be further emphasized in the remainder of the paper. We remind the reader that we are interested here in the mechanisms of sinking rather than the processes by which water masses are transformed. Water mass transformation is clearly taking place in regions of deep mixing even though substantial sinking may not be achieved in these regions (for instance, the transformed water may simply be transported away laterally).

1) LARGE-SCALE INTERIOR DOWNWELLING

Consider a region of the ocean interior with buoyancy loss to the atmosphere and deep convective mixing. If it is assumed that the large-scale interior flow is governed by planetary geostrophic dynamics, then the linear vorticity balance requires that any interior downwelling be balanced by a northward flow within the mixed layer:

$$v = \frac{fW}{\beta h}, \tag{8}$$

where W is the downward vertical velocity at the base of the mixed layer and h is the mixed layer depth. The total downward mass flux due to downwelling in the ocean interior is then

$$M_I = \frac{\beta h L_x L_y v}{f}, \tag{9}$$

where L_x and L_y are zonal and meridional length scales of the region of deep mixing and downwelling.

The total northward mass flux driven by the buoyancy loss is given by $M = vhL_x$. If the region of downwelling is confined to the latitude band of scale L_y, then linear vorticity dynamics require that the region of downwelling be connected to the western boundary by eastward and westward flowing zonal jets, as discussed by Pedlosky (1996) and Spall (2000). The circulation in the deep layer is of the same structure with opposite sign. The ratio of the interior sinking rate M_I to the recirculation strength M is given by

$$\frac{M_I}{M} = \frac{\beta L_y}{f}. \tag{10}$$

For high-latitude basins with deep mixing confined to regions O(500 km) in meridional extent, the interior sinking rate is an order of magnitude less than the recirculation rate. Hence the amount of northward flow required to balance any interior downwelling greatly exceeds the resulting downward mass flux in the interior. The reason for this is that, within planetary geostrophic dynamics, the horizontal mass flux divergence results only from variations in f. For mixing regions smaller than the basin scale, f does not vary sufficiently to allow significant downwelling without inducing a very large horizontal circulation.

As was shown in the previous section, the introduction of a lateral boundary breaks this geostrophic constraint and gives rise to a large horizontal mass flux convergence and downwelling. The vorticity balance in this case is made clear by the boundary layer solutions of Spall (2000). For sufficiently narrow downwelling regions (on the order of the Munk or Stommel layer thickness, as found here), the vertical stretching induced by downwelling is exactly balanced by viscous fluxes into the boundary or bottom. Thus the strong horizontal recirculation gyres that are required in the ocean interior, that is, (10), are eliminated if the downwelling takes place near the boundary.

Send and Marshall (1995) found that the net downwelling over a small region of cooling in a nonhydrostatic model of convective plumes was neglegible. The downward mass flux of dense water carried in the small-scale plumes was balanced by upwelling of lighter water between the plumes. The convection sites are regions of a net vertical heat flux, but not of a net vertical mass

flux. They also used a potential vorticity balance to show that the amount of relative vorticity required to balance significant downwelling was unrealistically large. This is analogous to the above planetary geostrophic scaling that indicates an unrealistically large horizontal circulation would be required to balance a net downwelling on the large scale.

2) Baroclinic instability of convection sites

Net sinking may also be achieved through eddy thickness fluxes that break the planetary geostrophic constraint. If cooling is spatially variable and persists long enough, or if the ocean is appropriately preconditioned, a region of closed isopycnals may develop within the cooling region. The geostrophic adjustment to this horizontal density gradient gives rise to a rim current flowing around the dense water. For sufficiently large and strong regions of cooling, such rim currents can become baroclinically unstable. The resulting eddies transport heat laterally and vertically between the cooling region and the surrounding water. The heat flux carried by these eddies has been found to balance a net surface cooling in many laboratory and numerical modeling experiments (Visbeck et al. 1996). The release of potential energy coincident with the formation of the eddies results in a net sinking of the dense waters within the region of sloping isopycnals.

The net vertical mass flux carried by large amplitude eddies resulting from instabilities of baroclinic rim currents can be estimated using the theory of Visbeck et al. (1996). Consider a region of closed isopycnals at the surface, such as is found in the interior of the Labrador Sea in winter. The mixed layer h in the interior of the convective region is typically quite deep, while the surrounding area is generally lighter in density and experiences mixing down to a shallower depth. For convenience let us assume a two-layer fluid where the bounding interface outcrops over some closed region and descends to a depth h_1 surrounding the region of deepest mixing. The maximum downward mass flux carried by the eddies, M_E, will be found at the depth h_1 and will be equal to the net lateral mass flux into the convective region above h_1. The total vertical mass flux may then be written as

$$M_E = 2\pi L\overline{v'h_1'}, \tag{11}$$

where L is the radius of the convective region and $\overline{v'h_1'}$ is the eddy thickness flux toward the center of the convective region above depth h_1.

Visbeck et al. (1996) have used scaling arguments and baroclinic instability theory to estimate the lateral eddy heat flux in terms of the mean properties of the flow. This may also be expressed as a lateral mass flux when posed in terms of isopycnal layer thicknesses as

$$\overline{v'h_1'} = \frac{1}{2}c_e U h_1, \tag{12}$$

where c_e is a nondimensional constant and U is a velocity scale for the rim current. The velocity of the rim current can be estimated from geostrophy as $U = g\Delta\rho_E h_1/\rho_0 fL$, where $\Delta\rho_E$ is the density change across the region of closed isopycnals. Visbeck et al. (1996) have estimated empirically that $c_e \approx 0.02$ for a wide variety of numerical and laboratory experiments, while Spall and Chapman (1998) derived a theoretical estimate with an upper bound of $c_e \approx 0.04$.

The total vertical mass flux carried by baroclinic eddies M_E is then estimated as

$$M_E = \frac{\pi c_e g\Delta\rho_E h_1^2}{\rho_0 f}. \tag{13}$$

To compare this with the estimate for sinking due to boundary convection, we need to relate the depth of mixing outside the deepest convection site, h_1, to the depth of deepest convection h. For simplicity, we assume that $h_1 = h/2$, although the results are not qualitatively sensitive to this choice, recognizing that $h_1 < h$. The ratio of eddy-induced sinking to boundary sinking is then estimated to be

$$\frac{M_E}{M_B} = 2\pi c_e\frac{\Delta\rho_E}{\Delta\rho_B} \approx 0.1\frac{\Delta\rho_E}{\Delta\rho_B}. \tag{14}$$

The relative efficiency of the two processes scales directly with the change in density across the convective site compared to the change in density along the lateral boundary. The ratio of the sinking rates is independent of the length scales of either regime. Because the efficiency at which the instabilities transport heat (and mass) transverse to the mean flow is relatively low ($c_e \ll 1$) it takes an order of magnitude more density contrast across the convective sites than along a lateral boundary to achieve the same amount of sinking.

These results suggest that it is very difficult to get water to sink in regions of deep mixed layers in the open ocean. By contrast, modest density changes along a lateral boundary resulting from surface cooling leads to significant downward mass flux. Estimates of sinking rates from these three mechanisms based on observations within the Labrador Sea are discussed in section 5.

3. Downwelling in a model ocean

In order to demonstrate the importance of the boundary sinking process to the thermohaline circulation, we diagnose the amplitudes and regions of downwelling in a simple numerical model of the wind- and buoyancy-driven circulation and compare the model results to the theory developed in section 2. Further discussion of the horizontal and overturning circulations, and their dependence on the downwelling dynamics, is given in section 4.

a. Model description

The model used in this study is the level coordinate, primitive equation model MOM2 (beta version 2.0) de-

scribed by Pacanowski (1996). The model solves the primitive equations of motion on a spherical grid making use of the hydrostatic, Boussinesq, and rigid-lid approximations. Each of the model calculations presented here is carried out at relatively low resolution so that hydrostatic instabilities and the generation of mesoscale eddies are suppressed. For simplicity, temperature is the only thermodynamically active tracer and a linear equation of state is employed. Individual convective plumes and nonhydrostatic processes in the vertical are not resolved. We focus this initial study on the large-scale manifestations of the downwelling regimes in order to provide a simple, intuitive framework from which to proceed into physically more complex systems.

The model domain is an ocean sector 50° wide that extends from 20°S to 60°N. The horizontal resolution is either 1.2° or 2°. The vertical discretization uses 24 levels with spacing increasing from 25 m near the surface to 308 m near the bottom. The maximum basin depth is 4000 m. Calculations have either a flat bottom or an idealized sloping bottom near the coasts (discussed further below). Each of the model calculations has been carried out for a period of 1000 years. All results are derived from mean fields over the final 250 years of integration, although there remains low-frequency variability in some cases with bottom topography. We emphasize two model configurations in the discussion because they illustrate the importance of convective activity near the subpolar boundaries on the structure of the subpolar gyre. We note, however, that the mean circulation both with and without topography are also dependent on a number of additional parameters that are not varied here.

Subgridscale processes are parameterized by a Laplacian horizontal viscosity (coefficients 4×10^8 cm^2 s^{-1} and 8×10^8 cm^2 s^{-1} for the 1.2° and 2° runs, respectively) and second-order vertical viscosity and diffusivity (coefficients 1 cm^2 s^{-2}). The dynamic boundary layers are well resolved in these calculations because the grid spacing resolves the viscous Munk layer. There is no bottom drag in the model, although calculations with nonzero bottom drag have been carried out and are qualitatively similar to those reported here.

The treatment of subgridscale parameterizations for temperature requires a little more discussion. The horizontal diffusion of temperature has been set to zero. The effect of mesoscale eddies is parameterized through the eddy-induced advective velocity following the approach of Gent and McWilliams (1990) with an along-isopycnal thickness diffusion coefficient of 10^7 cm^2 s^{-1}. For the linear equation of state used here, there should be no diffusion of temperature along an isopycnal surface. However, the finite difference approximation to the isopycnal rotation does result in some amount of temperature diffusion and smoothing. We present results here using along-isopycnal diffusion with a coefficient of 10^7 cm^2 s^{-1}. This coefficient is reduced in regions of isopycnal slopes greater than 0.01 using a hyperbolic tangent function [see Pacanowski (1996) for details] so that within the mixed layer, where the isopycnals are vertical, the diffusion is zero. We find noisier solutions, and significant large-scale differences in the subpolar gyre, in calculations with the along-isopycnal diffusion explicitly set to zero (particularly in the flat bottom case, discussed further below). However, the general relationship between the regions of downwelling and their dependence on boundary convection (the main points addressed in this paper) remain unchanged. Furthermore, we have calculated the along-isopycnal diffusion term in the temperature equation and find that the advective/convective balance used to derive the cooling spiral in section 2 is dominant in the mixed layer of the model.

The model is forced at the surface with an idealized zonal wind stress representing the southern and northern tropical gyres, the subtropical gyre, and the subpolar gyre, as indicated in Fig. 1. Buoyancy forcing is also included at the surface through a restoring term on temperature. The restoring timescale is varied between 30 days and 240 days, and is 120 days unless otherwise stated. This is equivalent to a surface heat flux of 10 W m^{-2} for a 1°C difference between the ocean and the atmospheric temperature. Although this restoring is weaker than has been typically used for ocean models, this value is within the recent estimate of 5 W m^{-2} K^{-1} to 15 W m^{-2} K^{-1} obtained by Seager et al. (1995) using an atmospheric boundary layer model that is allowed to adjust to SST anomalies. The effective atmospheric temperature to which the upper ocean is restored is shown in Fig. 1. The temperature decays from a maximum of 25° at the equator to a minimum of 3° in the northwest corner. At low latitudes there is only a slight east–west gradient, while at the latitudes of the subpolar gyre the east–west gradient is enhanced. An enhanced meridional gradient is also introduced near the western boundary between the wind-driven subtropical and subpolar gyres at 40°N. These effects are introduced to reflect the generally colder atmospheric conditions found along the northeast coast of North America in winter. Calculations are also carried out with a more traditional atmospheric temperature that is a function of latitude only by using the zonal average of the temperature in Fig. 1. The general results are not sensitive to this specific form of air temperature; however, the pattern of the net surface heat flux is more realistic with the colder atmosphere over the western subpolar gyre.

b. Comparison with theory

The deep downwelling in the model is found to take place where there is convective mixing adjacent to steep topography or a wall. Before considering the overturning streamfunction (discussed in detail in section 4b), we first demonstrate that the velocity structure and overturning rates near the northern boundary in the model are consistent with the theory developed in section 2.

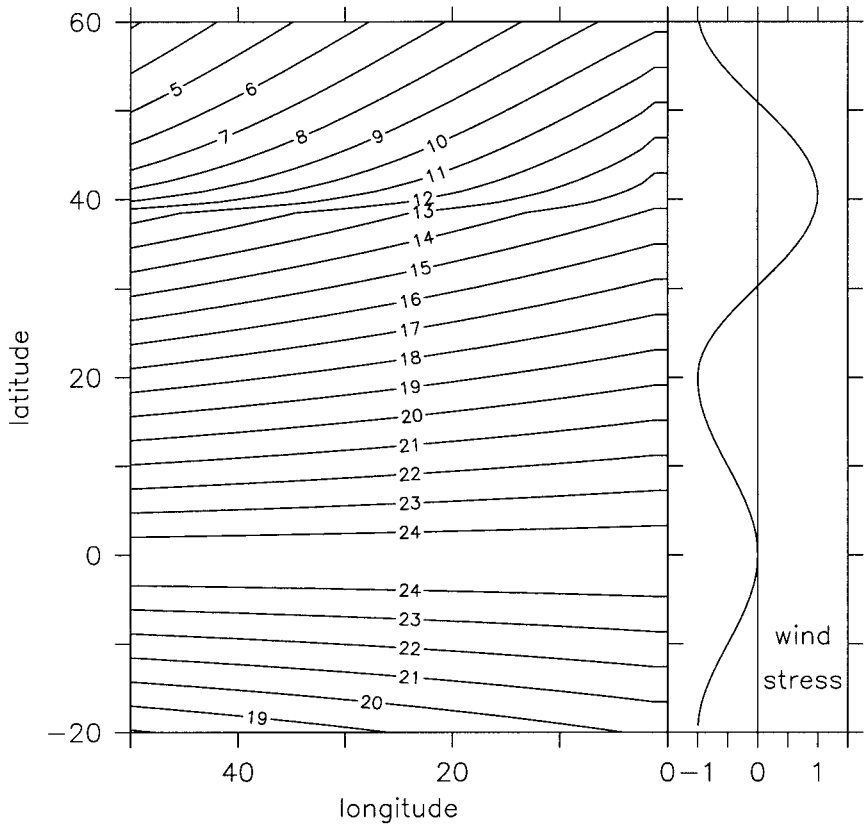

FIG. 1. Temperature toward which the model sea surface temperature is relaxed together with the meridional distribution of the zonal wind stress.

A typical velocity structure within the region of downwelling is indicated for a flat bottom calculation by the vertical profiles at 20°W shown in Fig. 2. The temperature is mixed uniformly down to a depth of approximately 2400 m (Fig. 2a). The vertical velocity increases downward from the surface to a maximum downwelling at a depth of 1200 m and then decreases to nearly zero by approximately 3000 m. The vertical velocity varies quadratically with depth within the mixed layer and is essentially zero below the mixed layer. The uppermost value of the vertical velocity is not zero (at depth 25 m) because of the Ekman transport into the northern wall. The vertical velocity one grid cell farther away from the boundary is essentially zero so that the vertical motion is confined to the narrow region adjacent to the boundary.

The horizontal velocities are shown in Fig. 2b. The zonal velocity is eastward in the upper 1000 m and westwards below 1000 m. The meridional velocity is northward above 1200 m and southward between 1200 m and approximately 3000 m. The vertical velocity is a maximum at the same depth at which the meridional velocity passes through zero. The meridional velocity below the mixed layer is nearly zero while the zonal flow is to the west. The predicted meridional velocity resulting from the cooling spiral calculation in section 2 [Eq. (4) with the assumption that $Q = V\rho_x$, indicated by the short dashed line in Fig. 2b] compares nicely with the meridional velocity in the model. This close agreement is found even though it was assumed in deriving (4) and (6) that $|v/u| \ll 1$.

The horizontal velocity structure, together with the quadratic nature of the vertical velocity, indicates a local balance where the water northward flowing in the upper mixed layer sinks within the northernmost cell and is returned toward the south in the deeper half of the mixed layer. The sense of the velocity rotatation with depth is counterclockwise, consistent with the velocity structure predicted by the cooling spiral calculation in section 2. This same structure of the horizontal and vertical velocity is found all along the northern boundary within the mixed layer, as indicated by the zonal section of the vertical velocity one grid cell south of the northern boundary in Fig. 3. There is downwelling everywhere within the mixed layer, with the maximum downwelling rate found at a depth of $h/2$. The downwelling is nearly zero everywhere below the mixed layer. Clearly the strength of the downwelling—and hence the high-latitude overturning streamfunction—in this model calculation is determined by the cooling spiral and the meridional geostrophic flow into the northernmost grid cell.

For this flat bottom calculation, $\Delta\rho_B = 0.18$ kg m^{-3},

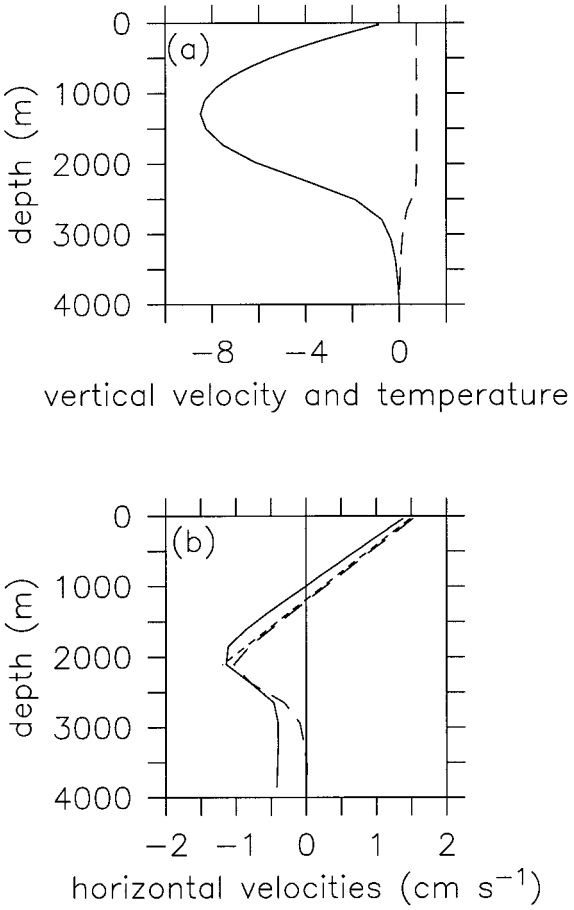

FIG. 2. Vertical profile at 20°W one grid point from the northern boundary: (a) vertical velocity (10^{-3} cm s^{-1} solid line) and temperature anomaly (relative to the bottom temperature, dashed line) and (b) zonal velocity (cm s^{-1} solid line) meridional velocity (cm s^{-1} dashed line).

$h = 3150$ m, and $f = 1.26 \times 10^{-4}$ s^{-1}, resulting in $M_B = 17$ Sv (Sv $\equiv 10^6$ m^3 s^{-1}). The density change $\Delta\rho_B$ is that between the northeast and northwest corners and the mixed layer depth h is the zonal average of the model mixed layer depth one grid point south of the northern boundary. This theoretical estimate compares reasonably well with the actual, non-Ekman sinking rate of 20 Sv found in the model. (The Ekman sinking rate is that resulting from the Ekman transport in the uppermost model level flowing into the northern boundary and downwelling, approximately 4 Sv for this wind stress and basin size.)

c. Parameter sensitivities

While the flat bottom calculation was found to agree reasonably well with the theory, it is important to investigate the sensitivity of the overturning estimate M_B to various parameters, including vertical mixing, air–sea exchange, bottom topography, and wind stress. For computational efficiency the horizontal resolution for these calculations is 2°, while the vertical resolution, model domain, and atmospheric temperature are all identical to the previous 1.2° calculation. The magnitude of the overturning rate is not very sensitive to the change in horizontal resolution. These calculations are intended to demonstrate the applicability of the theory derived in the preceeding section to a wide variety of parameter and flow regimes.

The maximum overturning streamfunction north of 50°N, minus the Ekman-driven sinking, is shown in Fig. 4 for a series of model calculations. The central calculation uses the same model parameters as the previous flat bottom 1.2° case but includes bottom topography that slopes exponentially upward toward the northern, eastern, and western boundaries to a minimum depth of 1730 m with an *e*-folding scale of 5° (indicated in Fig. 4 by the black diamond). The sensitivity of the overturning rate to bottom topography is indicated by the squares. A flat bottom calculation increases the overturning rate to approximately 20 Sv (seen above), while decreasing the bottom depth along the boundary from 1730 m to 1095 m to 500 m decreases the maximum overturning rate from 13 Sv to 6 Sv to 3 Sv. This decrease agrees well with the overturning estimate from the theory. The primary reason that the overturning decreases is that the mixed layer does not penetrate as deeply when the bottom topography extends higher into the water column along the northern boundary. This is due to both changes in the horizontal circulation and the presence of the bottom prohibiting further mixing. While the maximum overturning streamfunction suggests rather drastic changes in the thermohaline circulation, these are confined to the subpolar region. The overturning and meridional heat transport at mid and low latitudes is largely unchanged by bottom topography (see section 4). The rest of the parameter sensitivity calculations all use the bottom topography that extends to 1730 m along the boundary (compare the following results to the black diamond in Fig. 4).

The sensitivity of the maximum overturning rate to variations in the vertical diffusivity are indicated in Fig. 4 by the triangles. Decreasing the vertical diffusivity by an order of magnitude to 0.1 cm^2 s^{-1} results in a reduction of the overturning strength to 6 Sv, while increasing the diffusivity to 5 cm^2 s^{-1} results in an overturning of 12 Sv. Although these calculations are not in thermodynamic equilibrium, this increase in overturning strength with increasing diffusivity is consistent with previous studies (i.e., Marotzke 1997; Bryan 1987; Zhang et al. 1999; Colin de Verdiere 1988) and is reflected in our diagnostic by an increase in the average mixed layer depth along the northern boundary (1555 m compared to 1060 m).

The timescale over which the sea surface temperature is relaxed to the atmospheric temperature has also been varied from 30 days to 60 days to 240 days (asterisks in Fig. 4). The overturning rate increases with decreasing timescale, as expected, although the sensitivity of

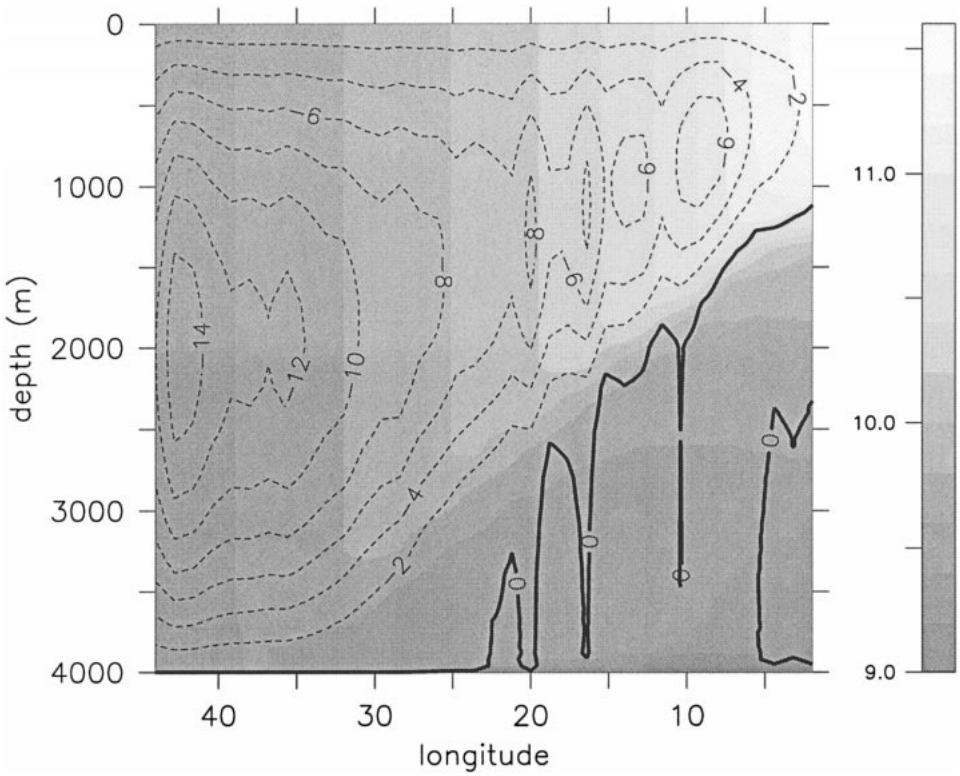

FIG. 3. Zonal section of vertical velocity one grid point from the northern boundary (10^{-3} cm s^{-1}) together with temperature (shaded).

the overturning rate is small as the timescale decreases below 120 days (the standard case).

Two additional calculations have been carried out with a flat bottom and a 30-day restoring timescale.

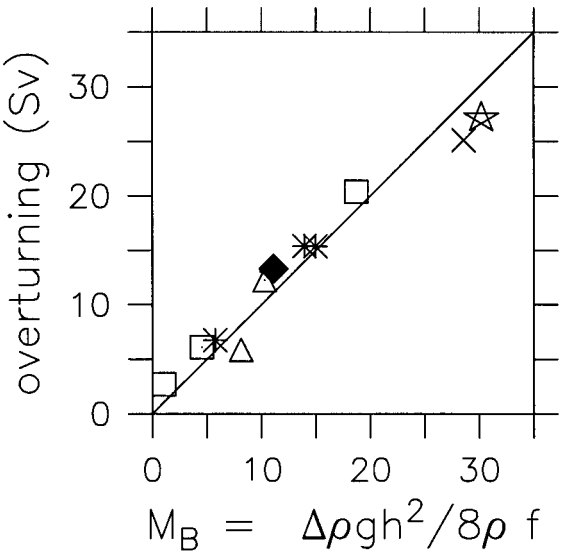

FIG. 4. Comparison of the non-Ekman component of the meridional overturning streamfunction with the theoretical estimate (7). The symbols correspond to various parameter sensitivity studies, as described in the text.

These cases are typical of what is usually used for climate studies and were chosen to test (7) in a strong overturning regime. The first case used the standard atmospheric temperature but had no wind stress (indicated by the cross). The second case used the standard wind stress but relaxed the sea surface temperature to the zonal average of the atmospheric temperature in Fig. 1 (star). In both cases the maximum overturning exceeds 25 Sv and is reasonably well predicted by (7).

We have not sought to conduct an extensive exploration of parameter space here. However, our results suggest that the dominant high-latitude downwelling mechanism in the model ocean is associated with convection adjacent to the boundaries. The theory developed in the previous section does a reasonably good job of reproducing the downwelling rate over a wide range of model parameters and overturning amplitudes when the mixed layer depth and density change along the boundary are diagnosed from the model calculations.

4. Circulation in the subpolar gyre

The parameter sensitivity studies in the previous section indicate that the strength of the high-latitude overturning streamfunction is very sensitive to the presence of topography near the boundaries. In this section we explore this sensitivity and its consequences for the large-scale horizontal circulation and hydrographic

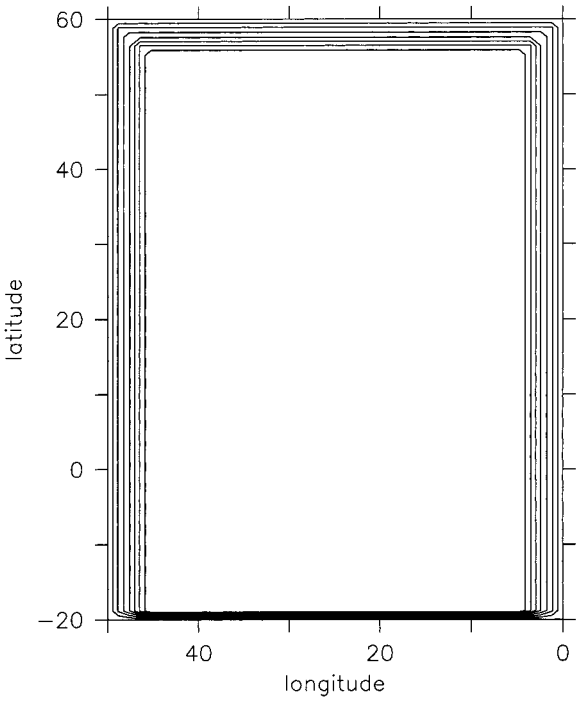

FIG. 5. Bottom topography with minimum depth of 1000 m and linear decay away from the boundaries (contour interval 500 m).

structure of the subpolar gyre. Specifically, we compare results from a 1.2° model with a flat bottom to that containing bottom topography that slopes linearly upward toward the boundaries over a horizontal scale of 5° (to a minimum depth of 1000 m, Fig. 5).

a. Horizontal circulation

The horizontal circulation and temperature at model level 2 (38.7 m) are shown in Fig. 6a for the flat bottom calculation. We focus on both the subpolar and subtropical gyres north of 20°N. The subtropical gyre is evident as a large-scale anticyclonic circulation in the velocity field while the horizontal flow in the subpolar gyre is generally northeastward and weak. Although the meridional flow is northward over most of the subpolar gyre, there is no evidence of cyclonic wind-driven flow in the near-surface circulation. As will be shown later, the depth-integrated circulation is indeed cyclonic, consistent with the wind forcing, but the westward flow at high latitudes is confined to the deep ocean. The coldest waters are found along the boundary in the northwest corner.

The mixed layer depth for the flat bottom calculation is shown in Fig. 6b (defined here as the depth at which the temperature decreases by 0.5° from its surface value). The mixed layer deepens as the northern boundary is approached with values increasing from approximately 1000 m in the northeast corner down to the the bottom in the northwest corner. Because the warm west-

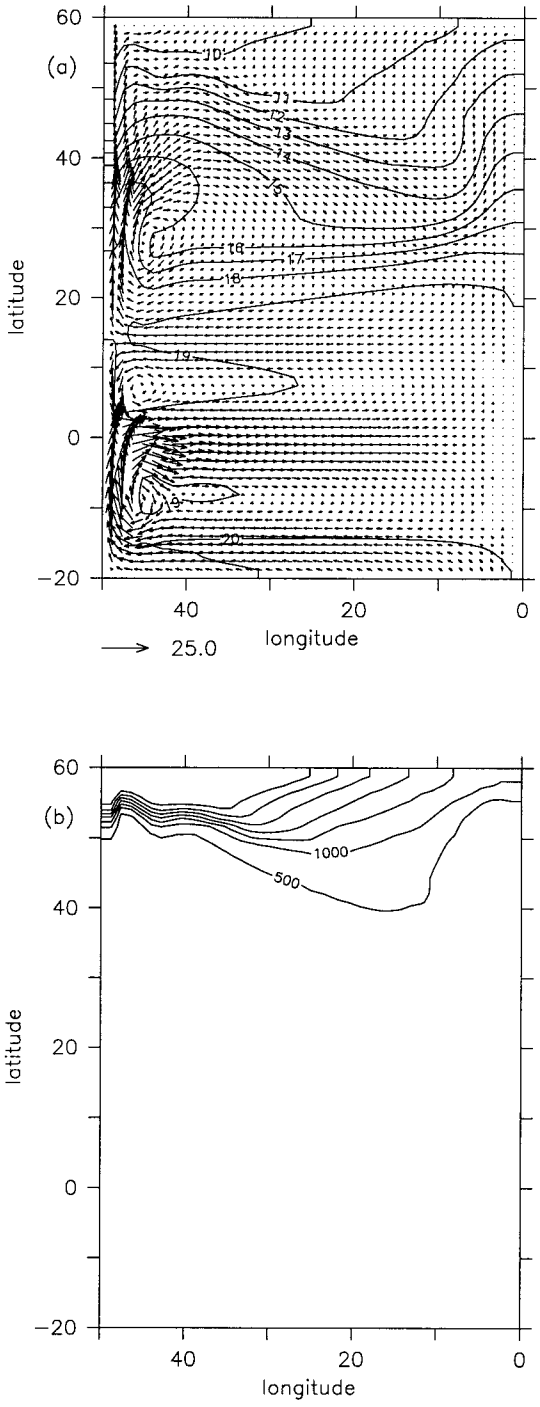

FIG. 6. (a) Temperature and horizontal velocity at 38-m depth and (b) mixed layer depth for the flat bottom calculation.

ern boundary current surface waters penetrate far into the subpolar domain along the western boundary, the western central subpolar gyre is strongly stratified with mixed layer depths less than 500 m.

The circulation in this flat bottom case is very idealized and contains fundamental differences when com-

pared to the observed circulation within the North Atlantic subpolar gyre (see, e.g., Talley and McCartney 1982; Schmitz and McCartney 1993). The densest surface waters in the North Atlantic are found in the gyre interior, not on the boundary as is found in the flat bottom model. The maximum mixed layer depths are also found in the western interior of the basin. In addition, the flow along the northern and western boundaries in the North Atlantic subpolar gyre is strong and circulates cyclonically around the basin perimeter, while the upper-layer flow in the model is weak and toward the northeast, even along the northern boundary.

Many of the obvious deficiencies of the horizontal flow and stratification found in the flat bottom calculation are removed with the addition of bottom topography. The horizontal velocity and temperature at model level 2 (38.7 m) for this case are shown in Fig. 7a. One immediately notes the presence of a robust subpolar gyre with a separated western boundary current between the subtropical and subpolar gyres that is stronger and sharper than was found with a flat bottom. The flow along the northern boundary is carried in a relatively strong westward flowing jet with velocities O(15 cm s^{-1}). This stronger westward velocity along the northern boundary is in part due to the shallow topography because the westward wind-driven flow must be carried over a shallower depth range. However, it is also intensified because the strength of the horizontal cyclonic circulation is increased as a consequence of sinking over bottom topography and stretching in the barotropic vorticity equation. The width of the rim currents are determined by the viscous boundary layer width and not the bottom topography. A similar dependence of the subpolar gyre circulation on the presence of bottom topography was found by Winton (1997).

One of the biggest changes found with the introduction of bottom topography is the reversal of the unrealistic eastward surface flow found in the northern boundary region. This is consistent with a simple scaling relationship (given in appendix A) that relates the amplitude of the velocity rotation over the depth of the mixed layer to the relative amplitudes of the horizontal and overturning circulations in the subpolar gyre. When the overturning circulation is large, as found for the flat bottom case, the total change in flow direction is large and the near-surface flow along the northern boundary will be toward the east. When the overturning circulation is relatively weak, as in the case with bottom topography, the total change in flow direction is small and the flow in the northern boundary current will be everywhere westward.

Relatively light waters are advected northward in the eastern basin and westward along the northern boundary by the strong boundary currents over topography. This results in the densest waters being found in the central western subpolar gyre, as is observed in the ocean [McCartney and Talley (1982) and Fig. 9]. Recall that with a flat bottom the densest waters were found on the boundary in the northwest corner of the basin. The SST in the western subpolar gyre is more than 4°C colder for the calculation with topography compared to that with a flat bottom (although the minimum temperature is similar in both cases). By contrast, the eastern basin

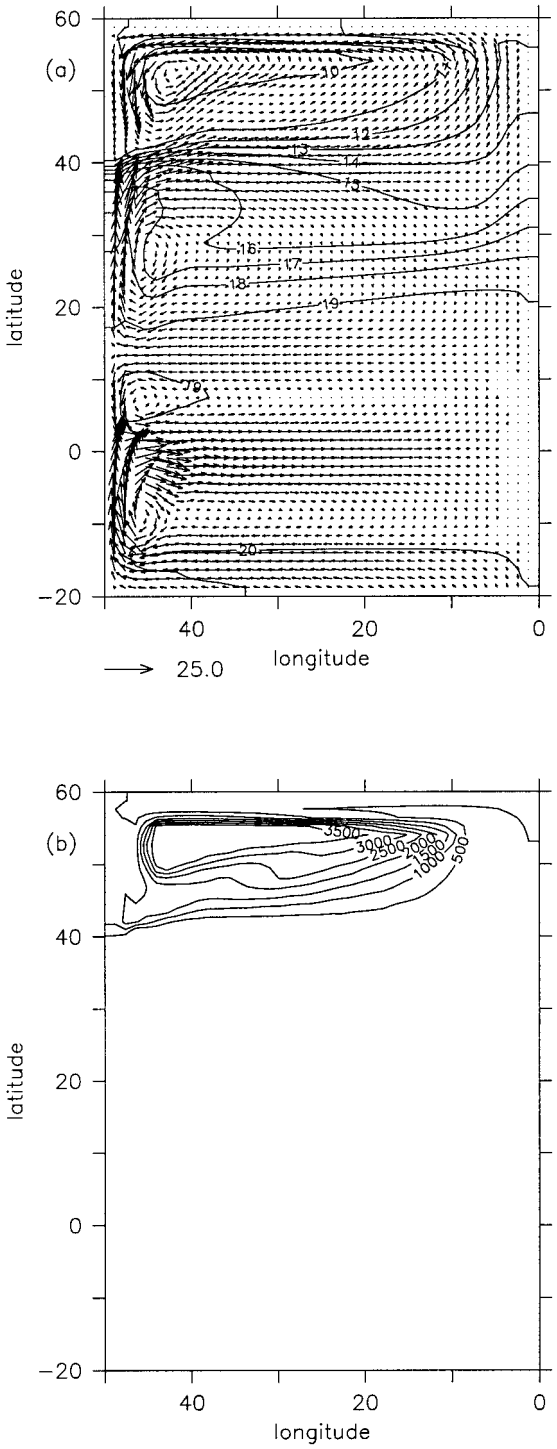

FIG. 7. (a) Temperature and horizontal velocity at 38-m depth and (b) mixed layer depth for the calculation with bottom topography.

and northern boundary current region are 1°–2°C warmer with topography.

Because the model Gulf Stream now separates from the boundary near 40°N, the lateral advection of heat (required to offset buoyancy loss to the atmosphere) is small in the central subpolar gyre and the most dense waters are found there. The surface heat flux is, in fact, strongest over the Gulf Stream and along the northern and western boundaries, precisely because this is where the lateral advection of warm waters is greatest. Surface fluxes are smaller in the interior even though this is where the surface density is greatest [consistent, e.g., with observations in the Labrador Sea; Lab Sea Group (1998)]. The mixed layer depth is also a maximum in the central western subpolar gyre (Fig. 7b). The net heat loss at the surface within the region of closed isopycnals is balanced by relatively weak lateral advection $O(1\text{ cm s}^{-1})$. The flow across isopycnals at the surface is possible because of the barotropic component of the flow. The eddy flux parameterization of cross-isopycnal heat transport is small, consistent with the scaling in section 2b. The meridional heat transport within the subpolar gyre is now carried primarily by the horizontal gyre rather than the overturning circulation that dominates the heat transport in the absence of strong rim currents.

The mixed layer depth is reduced along the northern and western boundaries by two mechanisms (which are not independent). The shallow topography limits the depths to which mixing can occur along the northern boundary. However, the rapid advection of lighter, stratified waters from the eastern basin into the northern boundary current also inhibits very deep convection from taking place within the boundary currents, although convection does occur.

Topography is not the only means by which such cyclonic boundary currents can be supported. A calculation with a flat bottom and zero isopycnal diffusion produces a circulation and mixed layer depth that resembles the case with topography. A similar circulation has also been obtained in a planetary geostrophic model with a flat bottom and weak diffusion by Samelson and Vallis (1997). The essential mechanism is the same in each case: lateral boundary currents advect light water around the perimenter of the basin and limit deep convection near the boundaries. With very little diffusion, the standard flat bottom calculation still has sufficiently strong boundary currents to restratify the near-boundary region. In our model, topography acts as an agent to enhance the boundary current strength in the presence of diffusion by increasing the depth-integrated cyclonic circulation in the subpolar gyre through JEBAR (joint effect of baroclinicity and relief). Although the model circulation is sensitive to the specific model configuration, the important point here is that, for any particular configuration, the downwelling is controlled by the convective activity near the boundaries.

The importance of convection adjacent to a boundary is emphasized by a flat bottom calculation (not shown) in which the near-boundary region (outermost four grid cells) was insulated to surface cooling. The circulation, sea surface temperature, mixed layer depth, and overturning in this case are similar to that found with topography and quite different from the standard flat bottom case. The reverse situation, insulating the interior of the subpolar gyre and cooling only over the four outermost grid cells, results in a circulation that looks much like the standard flat bottom case. These experiments support the interpretation that, if mixing near the boundaries is reduced, by whatever means, the dense waters cannot sink as deep at high latitudes. Each of the basic changes in the circulation and heat transport throughout the subpolar gyre follow as a direct consequence of this alteration in sinking patterns.

b. Meridional overturning

The meridional overturning for the flat bottom calculation at 1.2° resolution is shown in Fig. 8a. The wind-driven gyres are visible in the upper several hundred meters. The maximum overturning rate is 24 Sv and found at approximately 900-m depth. Essentially all of this sinking takes place adjacent to the northern boundary with upwelling found throughout most of the abyssal basin. This is consistent with the overturning found in most previous idealized models of the thermohaline circulation. A weak counterrotating deep gyre is found at low latitudes. Most of the water that ultimately sinks at high latitudes has been transported northward below the surface layer, although approximately 3 Sv flows downward out of the uppermost grid cell adjacent to the northern boundary. This small shallow mass flux is due primarily to the Ekman transport in the uppermost model level being forced into the northern boundary. The part relevant to this study is the remainder of the overturning circulation that is carried northward primarily below the Ekman layer, within the main thermocline, before sinking.

The overturning streamfunction for the calculation with topography is shown in Fig. 8b. The maximum overturning rate of approximately 13 Sv is found near 32°N. The upwelling at low latitudes is very similar to the flat bottom case. This is consistent with previous studies that have found a one-dimensional balance at low latitudes between upward heat advection and downward heat diffusion (the low-latitude stratification is similar in both model calculations). However, the sinking in the subpolar gyre is greatly reduced. This is as expected based on the mixed layer depth distribution shown in Fig. 7b and the theory presented in section 2. There are two latitude bands where significant downwelling takes place: 35°–45°N and north of 55°N. The sinking at latitudes between 35° and 45°N is occuring where the western boundary currents meet along the boundary. This is the adiabatic subduction of the deep western boundary current under the Gulf Stream discussed by Hogg and Stommel (1985). This southward

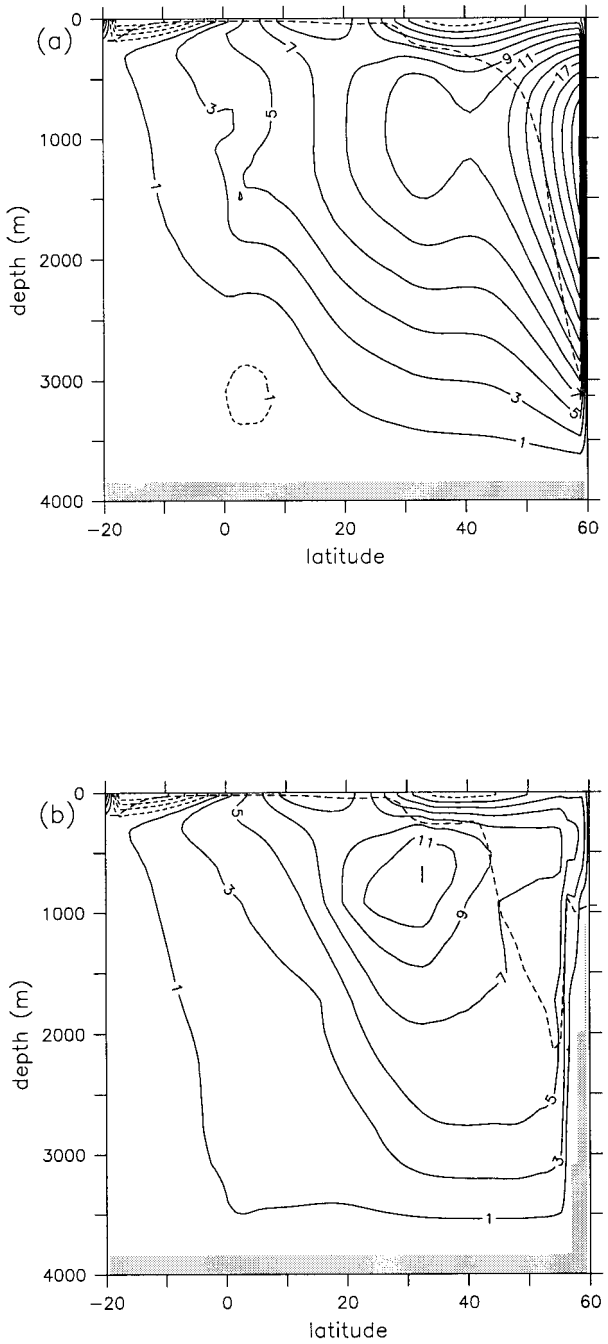

FIG. 8. The meridional overturning streamfunction (Sv) for (a) a flat bottom and (b) a continental slope. The dashed line indicates the depth of the zonally averaged mixed layer

shift in the maximum overturning (compared to the flat bottom case) is a direct consequence of the dynamics that control sinking at high latitudes. Because these cold boundary current waters do not sink, even along the boundaries of the subpolar gyre, they remain high in the water column until they reach the Gulf Stream. An important consequence of this dense water flowing southward near the surface (as opposed to flowing southward at great depth) is that the Gulf Stream separation latitude is shifted toward the south (Figs. 6a and 7a; Spall 1996). We may expect similar dynamics to be active in other regions where cold and warm western boundary currents meet (i.e., near the Grand Banks in the North Atlantic).

The sinking north of 55°N is taking place where deep mixing is found adjacent to topography. The total sinking north of 50°N is approximately 8 Sv, with 3 Sv due to Ekman transport into the northern boundary and 5 Sv due to buoyancy forcing. Most of this non-Ekman-driven sinking takes place where the mixed layers reside adjacent to the deep topography (Figs. 5, 7b). From the density field we estimate that $\Delta\rho_B = 0.1$ kg m^{-3} and $h = 2000$ m (the zonal average of h at latitude 55°N, where the deep mixing is adjacent to steep topography). The theoretical estimate (7) then gives $M_B = 4$ Sv, close to the non-Ekman sinking found in Fig. 8b.

Some of the downwelled western boundary current water in our model was formed in the northern rim current, while some was formed within the center of the subpolar gyre and advected into the western boundary region by a weak horizontal advection. These two ventilation processes involve very different timescales and occur in different regions of the ocean. We can expect that any changes in the atmospheric forcing conditions that alter the properties of the waters formed in the boundary currents of the subpolar gyre will be advected to low latitudes much more quickly than will any changes that are imprinted on the water masses in the interior of the gyre. This is in line with the observations of Pickart et al. (1997).

We emphasize again the distinction between water mass transformation and sinking. The densest waters and deepest mixed layers are formed in the subpolar gyre interior, between 50° and 55°N, but the net sinking there is nearly zero. Deep mixing alone is not an indicator of downwelling and meridional overturning. The area of deep mixed layers (greater than 1000-m depth) is over 50% larger in the case with bottom topography than it is in the case with a flat bottom. Yet the maximum high-latitude overturning circulation in the subpolar gyre for the calculation with topography is only about 25% of that found with a flat bottom. This is because the strong boundary currents cause the regions of deepest mixing to occur in the basin interior, where the large-scale dynamics of planetary geostrophy apply.

5. Observational estimates of boundary sinking

Recent observations have, for the first time, documented that deep convection can occur within a strong boundary current (Pickart and Torres 1998). This is contrary to the historical notion that such overturning is largely confined to the center of closed gyres, such as the Greenland gyre (Swift and Aagaard 1981) and Labrador gyre (Lazier 1973; Clarke and Gascard 1983). While indirect evidence has suggested that significant

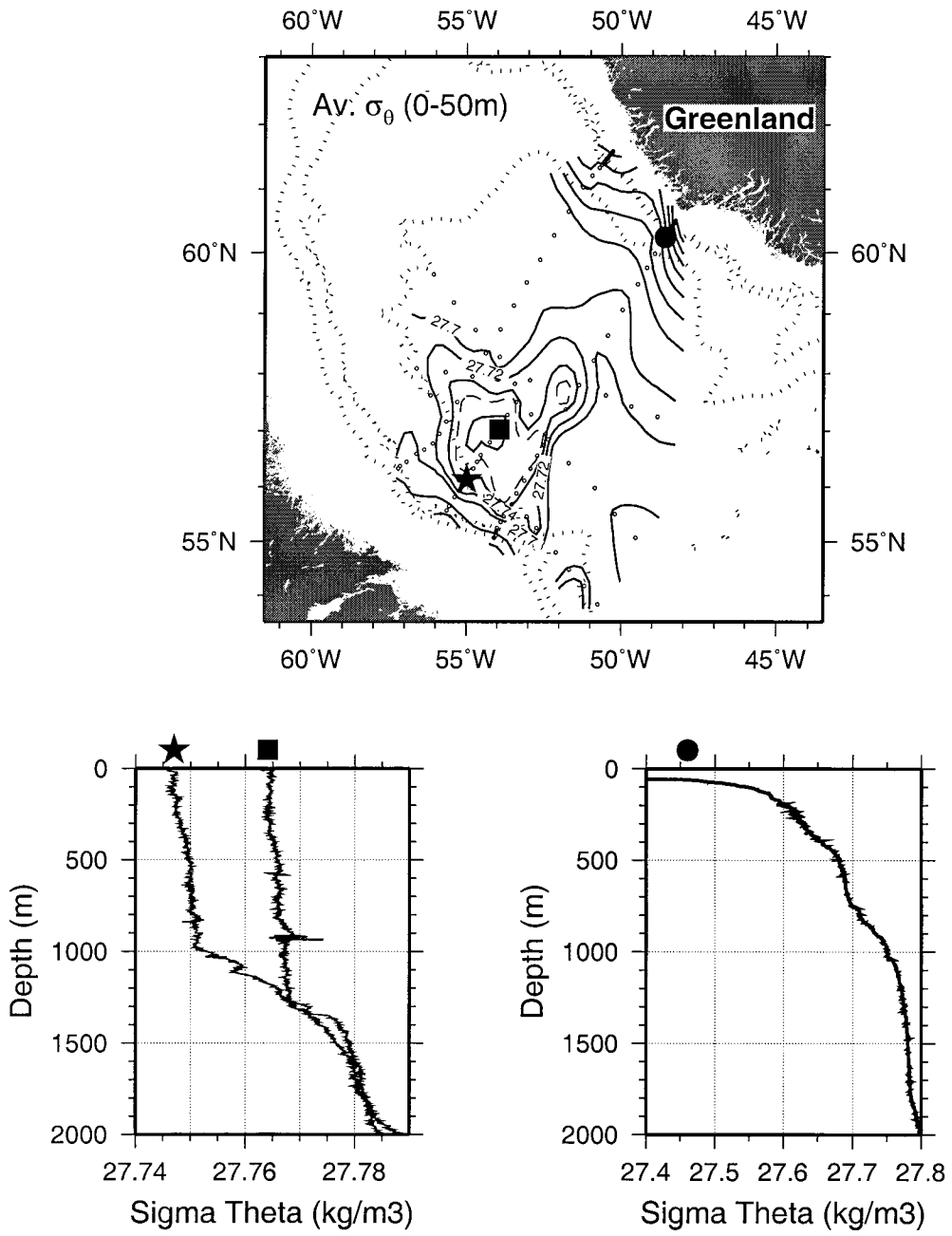

FIG. 9. (upper) Average potential density in the upper 50 m from the 1997 Labrador Sea winter hydrographic survey (Lab Sea Group 1998). The locations of the three stations are marked with bold symbols: western boundary (star), center of Labrador Sea gyre (square), and eastern boundary (circle). (lower) Potential density profiles for the three stations.

water mass transformation must be taking place adjacent to high-latitude boundaries (McCartney and Talley 1982; Mauritzen 1996; Pickart et al. 1997), direct observations of this process had been lacking.

As part of the Labrador Sea deep convection experiment in winter of 1997 (Lab Sea Group 1998), hydrographic and velocity measurements were obtained along both the western and eastern boundaries of the Labrador Basin. As expected, deep mixed layers were observed in the interior of the Labrador Sea cyclonic gyre, consistent with earlier measurements (Clarke and Gascard 1983; Wallace and Lazier 1988). However, mixed layers up to 1000 m deep were also measured in the western side of the boundary current system over the continental slope (Fig. 9). In general the mixed layers are warmer, saltier, lighter, and shallower along the slope than in the interior.

This is due to the fact that the boundary current is advecting warm and salty ''Irminger Water,'' a remnant of the Gulf Stream/North Atlantic Current. Interestingly, deep convection was not observed in the eastern (northward flowing) boundary current in the 1997 experiment, possibly due to the less intense atmospheric forcing on that side of the basin. However, Pickart et al. (2000) present evidence that boundary convection does indeed occur farther ''upstream'' as well, using data collected along the east Greenland continental slope.

We point out as well that significant mixed layer depths have been observed close to the northern boundary in the Gulf of Lions (Schott et al. 1996), suggesting that boundary convection might be occurring in the Mediterranean at the shoreward edge of the North Mediterranean Current. Godfrey and Ridgway (1985) describe a change in density along the west coast of Australia associated with buoyancy loss from the Leeuwin Current to the atmosphere, and infer that downwelling must be taking place in this region very close to the boundary.

As mentioned above, water mass transformation does not necessarily imply sinking, so it is of interest to apply the theoretical estimate for M_B to the 1997 winter dataset. Figure 9 shows density profiles from the western boundary, eastern boundary, and center of the Labrador gyre from the 1997 dataset. Note that, since convection was not occurring on the eastern boundary and we do not have data along the boundary between the eastern and western sections, there is some uncertainty in estimating the parameters $\Delta\rho_B$ and h. We calculate $\Delta\rho_B = 0.1$ kg m^{-3} as the difference in density between the eastern and western profiles averaged over the upper 1000 m. For $h = 1000$ m (see the western profile), (7) gives an M_B of 1 Sv. It should be noted that mixed layers along the boundary should occasionally extend deeper than this; for example, the profiles in Fig. 9 were collected in early March, and convection is observed to reach its maximum depth almost a month later (Lilly et al. 1999). Also, the mixed layers within the boundary current observed in 1991 analyzed by Pickart et al. (2000) extend to 1500 m. Using this value of h in (7) boosts the associated overturning to 2 Sv.

There have been other estimates of the rate of Labrador Sea Water formation; however, these earlier results generally did not distinguish between transformation and sinking, hence it is difficult to compare them directly to the sinking rate of 1–2 Sv obtained here. For example, Wright (1972) used heat flux estimates over the Labrador Sea in conjunction with climatological sea surface data to determine the volume of intermediate water formed, which implied an annual rate of 3.5 Sv. Clarke and Gascard (1983) computed a production rate quite similar to this using wintertime hydrographic data collected in 1976. However, inherent in both these calculations is the assumption that the entire volume of newly formed water within the Labrador gyre is flushed out each year. Speer et al. (1995) calculated a net transformation of approximately 1 Sv by integrating climatological sea surface fluxes over the different density classes found in the Labrador Sea. Worthington (1976) did explicitly depict sinking within the Labrador Sea, and estimated its magnitude using a box model encompassing the deep layer of the entire North Atlantic. Interestingly, Worthington's estimate of 2 Sv is comparable to the value presented here.

It is important to realize that all of the earlier estimates were inferred to take place in the interior of the Labrador Sea, to be contrasted with our sinking estimate which occurs near the boundaries. As noted in section 2b it is likely that any sinking in the interior is small compared to that occurring along the boundary. This can be quantified using the 1997 winter dataset as well. The eddy-driven sinking rate can be estimated by using the western boundary density profile and that for the gyre interior (Fig. 9). The ratio $\Delta\rho_E/\Delta\rho_B$ is found to be $O(0.1)$, giving $M_E/M_B \approx 0.01$. It has also been suggested that net sinking can take place on spatial scales of the region of deep mixing. The meridional scale of the interior deep mixed layer in Fig. 9 is $O(300$ km), which gives a ratio of large-scale interior sinking to baroclinic recirculation of $M_I/M = 0.05$. This means that to obtain sinking in the interior of order 1 Sv requires a baroclinic interior gyre of 20 Sv, far stronger than observed in 1997. This suggests that interior sinking in the Labrador Sea is indeed negligible.

Note, however, that our estimates do not necessarily contradict the earlier studies. The interior production rates noted above can be construed as water mass transformation. For instance, the water within the gyre may be transformed in the winter and then transported laterally either by advection or lateral diffusion. Our results suggest that a significant amount of the total production of Labrador Sea Water is able to sink locally within the Labrador Sea by boundary convection. However, it appears that the remainder of Labrador Sea Water is prohibited from sinking in this region because of the dynamics that control high-latitude interior downwelling.

6. Summary

The preceeding analysis and model results suggest that a dominant component of the downwelling limb of the thermohaline circulation takes place in regions where cooling occurs adjacent to lateral boundaries or steep topography. When large-scale flows are subject to cooling, geostrophic and thermodynamic balances require that the horizontal velocity vector within the mixed layer rotate counterclockwise with depth. The amplitude of downwelling that can occur in the large-scale open ocean, even in the presence of cooling, is strongly limited by planetary geostrophic dynamics. However, when cooling takes place near a lateral boundary, the boundary can support a lateral pressure gradient and break the constraints imposed by planetary geostrophic dynamics. The vorticity budget in such regions of narrow downwelling near a boundary are discussed by Spall (2000). A diagnostic estimate of the overturn-

ing rate resulting from boundary convection was derived to be

$$M_B = \frac{g\Delta\rho_B h^2}{8\rho_0 f}, \tag{15}$$

where M_B is the overturning rate, $\Delta\rho_B$ is the change in mixed layer density along the horizontal boundary, h is the average mixed layer depth along the boundary, g is the gravitational acceleration, ρ_0 is a reference density of seawater, and f is the Coriolis parameter. Scaling estimates indicate that sinking due to boundary convection is likely to dominate over sinking in the open ocean as well as sinking that results from baroclinic instability within deep convection sites.

We feel that the primary advantage of the approach taken here is that it is focused on the processes that control the downwelling rate and location. The relationship between sinking and the properties of the mixed layer near the boundaries allows one to infer the sinking rate directly from observations. The essential ingredients for active sinking near boundary regions are cooling and convective mixing along the boundary and an (not unrelated) along-boundary density gradient. Observations in the North Atlantic Ocean indicate that convection resulting from surface cooling does take place very close to the boundaries within the Labrador Sea and the Irminger Sea (Pickart et al. 1997; Pickart et al. 2000). This establishes a density gradient along the boundary of the same sign as found in the present model calculations and consistent with sinking along the boundary.

These results emphasize the importance of the rim current system and the stratification near the basin boundaries to the amplitude of downwelling and the basin-scale hydrography. This suggests that low-frequency variability of air–sea heat fluxes as well as the rim current strength may have a strong regulating effect on the low-frequency variability of the meridional overturning and horizontal circulations.

Acknowledgments. Support for this work was provided by the National Science Foundation through the Atlantic Circulation and Climate Experiment under Grant OCE-95-31874 (MAS) and the Office of Naval Research Grants N00014-97-7-1-0088 (MAS) and N00014-98-1-0043 (RSP). Constructive suggestions and questions by two anonymous reviewers also helped to clarify these results.

APPENDIX

Flow Direction at the Northern Boundary

The direction of the surface flow near the northern boundary may be related to the relative strengths of the horizontal and overturning circulations. For flows in which the total change in flow direction over the depth of the mixed layer is small, the zonal component of the flow in the northern boundary current will be everywhere westward. However for a sufficiently large velocity spiral the zonal flow may change sign somewhere in the water column. The total change in flow direction over the mixed layer depth may be written in terms of the high-latitude sinking rate M_B. If the velocity vector in the northern boundary current rotates more than 180°, thermal wind requires that the surface flow have an eastward component. This condition is satisfied when

$$\frac{M_B}{hL_xV} \approx \frac{M_B}{M_B + M_H} > \frac{\pi}{8}. \tag{A1}$$

The transport hL_xV will scale as the sum of the overturning and horizontal transports, $M_B + M_H$. If the velocity near the northern boundary is primarily due to the overturning circulation, then $M_B > M_H$ and the surface flow will be toward the east. On the other hand, if there is a strong horizontal component such that $M_H > O(8M_B/\pi)$, then the total change in flow direction over the mixed layer depth will be less than 180° and the surface flow is expected to be toward the west throughout the water column. For the flat bottom case, $M_B = 25$ Sv, $M_H = 30$ Sv, and $M_B/(M_B + M_H) > \pi/8$. This is consistent with the eastward surface flow found in the model. For the case with topography, $M_B = 5$ Sv, $M_H = 55$ Sv, and $M_B/(M_B + M_H) \ll \pi/8$. The condition for eastward flow is not satisfied, also in agreement with the westward surface flow along the northern boundary found in the model.

REFERENCES

Böning, C. W., W. R. Holland, F. O. Bryan, G. Danabasoglu, and J. C. McWilliams, 1995: An overlooked problem in model simulations of the thermohaline circulation and heat transport in the Atlantic Ocean. *J. Climate,* **8,** 515–523.

——, F. O. Bryan, W. R. Holland, and R. Döscher, 1996: Deep water formation and meridional overturning in a high-resolution model of the North Atlantic. *J. Phys. Oceanogr.,* **26,** 1142–1164.

Bryan, F., 1986: High-latitude salinity effects and interhemispheric thermohaline circulations. *Nature,* **323,** 301–304.

——, 1987: Parameter sensitivity of primitive equation ocean general circulation models. *J. Phys. Oceanogr.,* **17,** 970–985.

——, and W. R. Holland, 1989: A high-resolution simulation of the wind- and thermohaline-driven circulation in the North Atlantic Ocean. *Parameterization of Small-Scale Processes, Proceedings of the 'Aha Huliko' a Hawaiian Winter Workshop,* P. Müller and D. Hendersin, Eds., Hawaii Institute of Geophysics, 99–115,

Bryan, K., and M. D. Cox, 1967: A numerical investigation of the oceanic general circulation. *Tellus,* **19,** 54–80.

Clarke, R. A., and J. C. Gascard, 1983: The formation of Labrador Sea water. Part I: Large-scale processes. *J. Phys. Oceanogr.,* **13,** 1764–1778.

Colin de Verdiére, A., 1988: Buoyancy driven planetary flows. *J. Mar. Res.,* **46,** 215–265.

Dietrich, G., K. Kalle, W. Krauss, and G. Siedler, 1980: *General Oceanography, An Introduction.* 2d ed. John Wiley, 626 pp.

Döscher, R., C. W. Böning, and P. Hermann, 1994: Response of circulation and heat transport in the North Atlantic to changes in thermohaline forcing in norther latitudes: A model study. *J. Phys. Oceanogr.,* **24,** 2306–2320.

Gent, P. R., and J. C. McWilliams, 1990: Isopycnal mixing on ocean circulation models. *J. Phys. Oceanogr.,* **20,** 150–155.

Godfrey, J. S., and K. R. Ridgway, 1985: The large-scale environment of the poleward-flowing Leeuwin Current, Western Australia: Longshore steric height gradients, wind stresses and geostrophic flow. *J. Phys. Oceanogr.,* **15,** 481–495.

Hogg, N. G., and H. M. Stommel, 1985: On the recirculation between the deep circulation and the Gulf Stream. *Deep-Sea Res.,* **32,** 1181–1193.

Lab Sea Group, 1998: The Labrador Sea Deep Convection Experiment. *Bull. Amer. Meteor. Soc.,* **79,** 2033–2058.

Lazier, J. R. N., 1973: The renewal of Labrador Sea water. *Deep-Sea Res.,* **20,** 341–353.

Ledwell, J. R., A. J. Watson, and C. S. Law, 1993: Evidence for slow mixing across the pycnocline from an open-ocean tracer-release experiment. *Nature,* **364,** 701–703.

Lilly, J. M., P. B. Rhines, M. Visbeck, R. Davis, J. R. N. Lazier, F. Schott, and D. Farmer, 1999: Observing deep convection in the Labrador Sea during winter 1994–1995. *J. Phys. Oceanogr.,* **29,** 2065–2098.

Luyten, J., H. Stommel, and C. Wunsch, 1985: A diagnostic study of the Northern Atlantic subpolar gyre. *J. Phys. Oceanogr.,* **15,** 1344–1348.

Marotzke, J., 1997: Boundary mixing and the dynamics of three-dimensional thermohaline circulations. *J. Phys. Oceanogr.,* **27,** 1713–1728.

——, and J. R. Scott, 1999: Convective mixing and the thermohaline circulation. *J. Phys. Oceanogr.,* **29,** 2962–2970.

Mauritzen, C., 1996: Production of dense overflow waters feeding the North Atlantic across the Greenland-Scotland ridge. Part 1: Evidence for a revised circulation scheme. *Deep-Sea Res.,* **43,** 769–806.

——, and S. Häkkinen, 1999: On the relationship between dense water formation and the ''Meridional Overturning Cell'' in the North Atlantic Ocean. *Deep-Sea Res.,* **46,** 877–894.

McCartney, M. S., and L. D. Talley, 1982: The subpolar mode water of the North Atlantic. *J. Phys. Oceanogr.,* **12**, 1169–1188.

Pacanowski, R. C., 1996: MOM2 version 2.0 (beta) documentation user's guide and reference manual. Tech. Rep. 3.2, GFDL Ocean Group, 232 pp. [Available from NOAA/Geophysical Fluid Dynamics Laboratory, Princeton, NJ 08542.]

Park, Y. G., and K. Bryan, 2000: Comparison of thermally driven circulations from a depth-coordinate model and an isopycnal-layer model. Part I: Scaling-law sensitivity to vertical diffusivity. *J. Phys. Oceanogr.,* **30,** 590–605.

Pedlosky, J., 1996: *Ocean Circulation Theory*. Springer-Verlag, 435 pp.

Pickart, R. S., and D. J. Torres, 1998: Wintertime hydrography of the Labrador Sea during active convection. *Eos, Trans. Amer. Geophys. Union,* **79,** OS174.

——, M. A. Spall, and J. R. Lazier, 1997: Mid-depth ventilation in the western boundary current system of the sub-polar gyre. *Deep-Sea Res.,* **44,** 1025–1054.

——, D. Torres, and K. Lavender, 2000: Is Labrador Sea Water formed in the Irminger Basin? *Eos, Trans. Amer. Geophys. Union,* **80**, p. 536.

Polzin, K. L., J. M. Toole, and R. W. Schmitt, 1997: Spatial variability of turbulent mixing in the abyssal ocean. *Science,* **276,** 93–96.

Robinson, A. R., and H. M. Stommel, 1959: The oceanic thermocline and the associated thermohaline circulation. *Tellus,* **11,** 295–308.

Samelson, R. M., and G. K. Vallis, 1997: Large-scale circulation with small diapycnal diffusion: The two thermocline limit. *J. Mar. Res.,* **55,** 223–275.

Schmitz, W. J., and M. S. McCartney, 1993: On the North Atlantic circulation. *Rev. Geophys.,* **31,** 29–49.

Schott, F., and H. M. Stommel, 1978: Beta spirals and absolute velocities in different oceans. *Deep-Sea Res.,* **25,** 961–1010.

——, M. Visbeck, U. Send, J. Fischer, L. Stramma, and Y. Desaubies, 1996: Observations of deep convection in the Gulf of Lions, Northern Mediterranean, during the winter of 1991/2. *J. Phys. Oceanogr.,* **26,** 505–524.

Seager, R., Y. Kushnir, and M. A. Cane, 1995: On heat flux boundary conditions for ocean models. *J. Phys. Oceanogr.,* **25,** 3219–3230.

Send, U., and J. Marshall, 1995: Integral effects of deep convection. *J. Phys. Oceanogr.,* **25,** 855–872.

Spall, M. A., 1992: Cooling spirals and recirculation in the subtropical gyre. *J. Phys. Oceanogr.,* **22,** 564–571.

——, 1996: Dynamics of the Gulf Stream/Deep Western Boundary Current crossover. Part I: Entrainment and recirculation. *J. Phys. Oceanogr.,* **26,** 2152–2168.

——, 2000: Buoyancy forced circulations around islands and ridges. *J. Mar. Res.,* in press.

——, and D. C. Chapman, 1998: On the efficiency of baroclinic eddy heat transport across narrow fronts. *J. Phys. Oceanogr.,* **28,** 2275–2287.

Speer, K. G., H.-J. Isemer, and A. Biastoch, 1995: Water mass formation from revised COADS data. *J. Phys. Oceanogr.,* **25,** 2444–2457.

Stommel, H., 1961: Thermohaline convection with two stable regimes of flow. *Tellus,* **13,** 224–230.

——, 1979: Oceanic warming of western Europe. *Proc. Natl. Acad. Sci.,* **76,** 2518–2521.

Swift, J. H., and K. Aagaard, 1981: Seasonal transitions and water mass formation in the Iceland and Greenland Seas. *Deep-Sea Res.,* **28A,** 1107–1129.

Talley, L. D., and M. S. McCartney, 1982: Distribution and circulation of Labrador Sea Water. *J. Phys. Oceanogr.,* **12,** 1189–1205.

Visbeck, M., J. Marshall, and H. Jones, 1996: Dynamics of isolated convective regions in the ocean. *J. Phys. Oceanogr.,* **26,** 1721–1734.

Wallace, D. W. R., and J. R. N. Lazier, 1988: Anthropogenic chlorofluorocarbons in newly-formed Labrador Sea Water. *Nature,* **332,** 61–63.

Weaver, A. J., J. Marotzke, P. F. Cummins, and E. S. Sarachik, 1993: Stability and variability of the thermohaline circulation. *J. Phys. Oceanogr.,* **23,** 39–60.

Winton, M., 1997: The damping effect of bottom topography on internal decadal-scale oscillations of the thermohaline circulation. *J. Phys. Oceanogr.,* **27,** 203–208.

Worthington, L. V., 1976: On the North Atlantic circulation. *The Johns Hopkins Oceanogr. Stud.,* No. 6, 110 pp.

Wright, W. R., 1972: Northern sources of energy for the deep Atlantic. *Deep-Sea Res.,* **19,** 865–877.

Zhang, J., R. W. Schmitt, and R. X. Huang, 1999: The relative influence of diapycnal mixing and hydrologic forcing on the stability of the thermohaline circulation. *J. Phys. Oceanogr.,* **29**, 1096–1108.